Published on 29 September 2014. Downloaded by National Chiao Tung University on 21/07/2015 10:47:55.

Nanoscale

ROYAL SOCIETY OF CHEMISTRY

PAPER

View Article Online
View Journal | View Issue

Cite this: *Nanoscale*, 2014, **6**, 14280

Smart assembling of multi-scaled functional interfaces in thermoelectric Ga_2Te_3/Te hetero-nanocomposites†

Hsiu-Cheng Chang, Ming-Hsiu Chiang, Tsung-Che Tsai, Tsung-Han Chen, Wha-Tzong Whang and Chun-Hua Chen*

Received 20th May 2014,
Accepted 28th September 2014

DOI: 10.1039/c4nr02765e

www.rsc.org/nanoscale

We describe an innovative concept and facile approach in fabricating laterally assembled Ga_2Te_3/Te binary nanocomposite films, which comprise two-dimensional quasi-periodic Ga_2Te_3 nanoassemblies surrounded by interlocking highly-conductive Te single crystals for comprehensively establishing subnano- to micro-scaled multi-style versatile interfaces. The distinct Ga_2Te_3/Te nanocomposite film exhibits a power factor that is about 60 times higher than the reported conventional Ga_2Te_3 and Te materials, mainly due to the 2- to 3-order improved electrical conductivity and the comparable Seebeck coefficient.

Introduction

Heterogeneous nanocomposites, which imply nano-scaled alternations in composition and morphology along one or up to three dimensions, are now rapidly emerging to be an exciting new research topic with significant potential for developing innovative thermoelectric materials and devices.[1–3] The pioneering interfacial concepts and nanotechnologies of these remarkable findings are mainly based on the designation and fabrication of a variety of unusual functional interfaces or surfaces that are abundantly found in the nanocomposites, which potentially offer the additional degrees of freedom in independently modulating the three physically related thermoelectric parameters, namely, Seebeck coefficient (S), electrical conductivity (σ), and thermal conductivity (κ), for achieving a remarkable thermoelectric figure of merit, ZT, defined as $S^2\sigma T/\kappa$.

Massively introducing heterogeneous interfaces or surfaces has been widely utilized and proven to be a facile strategy to effectively reduce thermal conductivity *via* enhanced phonon scattering. For most of the less-controlled nanocomposites, only a limited amount of phonons can be scattered, generally resulting in unexpectedly high thermal conductivity. Nowadays, the concept has evolved into scattering phonons with all-length-scale mean free paths by forming interfaces with various dimensions and scales. In practice, Kanatzidis *et al.* realized the co-presence of atomic-scale defects, nano-scale precipitations and meso-scale grain boundaries in the sodium doped PbTe/SrTe nanocomposites, which could scatter phonons with a very wide range of the mean free path, leading to a greatly reduced lattice thermal conductivity, and thus the most encouraging ZT value of ~2.2 at 915 K.[4] In addition to the main function of phonon scattering, recent exhilaratingly theoretical predictions[5–8] and several practical cases[9–16] remarkably highlight another functions of the heterogeneous interfaces, namely the special energy-selective charge carrier scattering induced by energy band bending across the interface, which significantly enhance the Seebeck coefficient, while relatively modest decreases in the electrical conductivity can be achieved. The most amazing demonstration should be the case of $In_{0.53}Ga_{0.47}As/In_{0.53}Ga_{0.28}Al_{0.19}As$ super-lattices, in which the well-designed heterogeneous interfaces successfully decouple the electrical conductivity and the Seebeck coefficient to gain an outstanding ZT of ~1.5, evidently proving the role of the interfaces in raising the electron filtering effects, and subsequently such a strong anisotropic Seebeck effect.[5]

In this work, we have designed and successfully fabricated a series of laterally assembled thermoelectric nanocomposite films, which regularly couple Ga_2Te_3 nanoparticle assemblies and Te single-crystal networks, using pulsed laser deposition (PLD) with subsequent annealing. Gallium telluride (Ga_2Te_3), which exhibits a considerably high p-type Seebeck coefficient of ~800 μV K^{-1}, and more importantly, an unexpectedly low thermal conductivity (~0.5 W m^{-1} K^{-1}) caused by the spontaneous formation of atomic-scaled periodic two-dimension (2-D) vacancy planes,[17–19] is thus specially selected to be the

Department of Materials Science and Engineering, National Chiao Tung University, Hsin-Chu 30010, Taiwan, Republic of China. E-mail: ChunHuaChen@mail.nctu.edu.tw

† Electronic supplementary information (ESI) available: Structural investigations of the hetero-nanocomposite films formed at an annealing temperature of 225 °C for 12 h, 250 °C for 3 h, and 225 °C for 3 h are collected in Fig. S1–S3, respectively. Annealing temperature and time effects on the morphology, composition, crystallinity and thermoelectric property are shown in Fig. S4–S10. See DOI: 10.1039/c4nr02765e

This journal is © The Royal Society of Chemistry 2014

Published on 29 September 2014. Downloaded by National Chiao Tung University on 21/07/2015 10:47:55.

main matrix for achieving the present target. The 2-D defects induced insufficiently high electrical conductivity ($\sim 10^{-1}$ Sm^{-1}) of the intrinsic Ga_2Te_3, strongly suggesting the necessity of choosing a highly electrically conductive cooperating phase. Tellurium (Te) which possesses not only a comparable high p-type Seebeck coefficient (~ 400 μV K^{-1})[20,21] but, most notably, an excellent electrical conductivity (up to $\sim 10^3$ Sm^{-1}),[21,22] is deservedly considered to be the most promising candidate to collaborate with Ga_2Te_3.

The periodically alternated Ga_2Te_3 and Te phases, possessing an average block size of ~3 μm and ~500 nm, respectively, spontaneously form distinct pseudo-super-lattice periodic structures lying on the substrate. The estimated period density of ~2600 pairs per centimetre along the in-plane direction, which is the working direction in this work, indicates an extremely high density of heterogeneous interfaces embedded in the present nanocomposite, which provides the required structural conditions to prove the concept of heterogeneous nanocomposites. We anticipate that the skillful collaboration of Ga_2Te_3 and Te, as well as the generation of high-density and periodical heterogeneous interfaces could retain the primitively high Seebeck coefficients of both components. Regarding the phonon transport, because phonons with shorter, medium, and longer mean free paths could be respectively scattered by the repeatedly appearing 2-D vacancy planes in Ga_2Te_3 (atomic-scale), homogeneous Ga_2Te_3/Ga_2Te_3 interfaces (nano-scale), and heterogeneous Ga_2Te_3/Te interfaces (meso-scale), a desired low thermal conductivity can be realized. Finally, although the 2-D atomic defects and the largely introduced various interfaces would significantly suppress the electrical conductivity, the Te single crystals provide a number of alternative channels for smoothly transporting charge carriers, and thus a comparably high electrical conductivity and power factor can be achieved. This work demonstrated the practicability and potential applications of using this type of techniques and the resulting unique laterally assembled Ga_2Te_3/Te nanocomposite films to gain thermoelectric energy.

Experimental

Nanocomposite films fabrication

Commercial Ga_2Te_3 powders of 0.6 g were dry-pressed into pellets of 10 mm in diameter and 2 mm thickness. An insulated SiO_2 layer (~500 nm) was thermally grown on the Si substrate (2×2 cm^2). The fabrication of laterally assembled Ga_2Te_3/Te nanocomposite films was performed into two steps: first, an Q-switched Nd:YAG laser (Litron, LPY664) with a focused laser fluence of 8.3 J cm^{-2} (532 nm wavelength, 10 ns pulse duration, 8 mm in beam diameter, and 5 Hz repetition rate) was utilized to fabricate the Ga_2Te_3 nano-assembled films with a thickness of ~2 μm on the SiO_2/Si substrate at 25 °C under an Ar ambient pressure of 10^{-2} torr. The as-grown Ga_2Te_3 nanoassembled films were then annealed in a tube furnace under an ambient N_2 pressure of 0.2 torr to control the morphology of the laterally assembled Ga_2Te_3/Te nanocomposite films.

Structural analyses

The field-emission scanning electron microscopy (FE-SEM, JEOL JSM-6500) equipped with EDS was used to investigate the morphology and the chemical composition of the as-prepared laterally assembled Ga_2Te_3/Te nanocomposite films. The crystalline structure was characterized by X-ray diffraction (XRD, Bruker AXS D8 Discover) with CuKα radiation ($\lambda \sim 1.54$ Å) in a θ–2θ scan mode. The microstructure and element distribution were studied using a transmission electron microscope (TEM, JEOL JEM-3000F) with energy dispersive spectroscopy (EDS) mapping capabilities. The cross-sectional specimen for the TEM investigation was prepared by focused ion beam (FIB, FEI Nova 200). The surface states were acquired by X-ray photoelectron spectroscopy (XPS, Thermo VG 350).

Thermoelectric properties

The carrier concentration, mobility, electrical conductivity, and Seebeck coefficient are measured along the in-plane direction at room temperature. Four Au electrodes of 100 nm size were thermally deposited near the corners of the nanocomposite films for in-plane Hall, electrical conductivity, and Seebeck coefficient measurements. The carrier concentration and mobility were obtained in the van der Pauw configuration by a Hall system (Accent HL5500). The electrical conductivity was investigated by a standard dc four-terminal method. For the Seebeck coefficient measurement, a micro-heater was applied to generate a temperature difference of 3–15 K between the two electrodes of the specimen. Silver paste was used to glue thermocouples on the electrodes. The temperature and temperature differences (ΔT) were measured using calibrated thermocouples, whereas the resulting thermally induced Seebeck voltage (ΔV) was measured by voltage probes to acquire the Seebeck coefficient ($S = \Delta V/\Delta T$). The well-developed 3ω technique was applied to measure the cross-plane thermal conductivity. A SiO_2 layer with a thickness of 100 nm was sputtered on the nanocomposite film surface to form the sandwiched structure (SiO_2/nanocomposite films/SiO_2) for this measurement. The patterned Au/Cr electrodes prepared *via* the microlithography process on the top of the SiO_2 surface served to be a heater and a thermometer as well. All the measurements were taken in a vacuum chamber ($\sim 10^{-3}$ torr).

Results and discussion

SEM analysis of the as-deposited Ga_2Te_3 matrix shows that the room-temperature PLD process on SiO_2/Si substrates yields dense and highly periodic cracks, which isotropically segment the Ga_2Te_3 matrix into approximately isolated pieces of micro-scaled irregular columns (Fig. 1a–c). The puzzle-like complementary boundaries between the neighbouring columns (Fig. 1a and b) as well as the wedge-shaped profile of the cracks (Fig. 1c) evidently indicate that the interlocking cracks

Published on 29 September 2014. Downloaded by National Chiao Tung University on 21/07/2015 10:47:55.

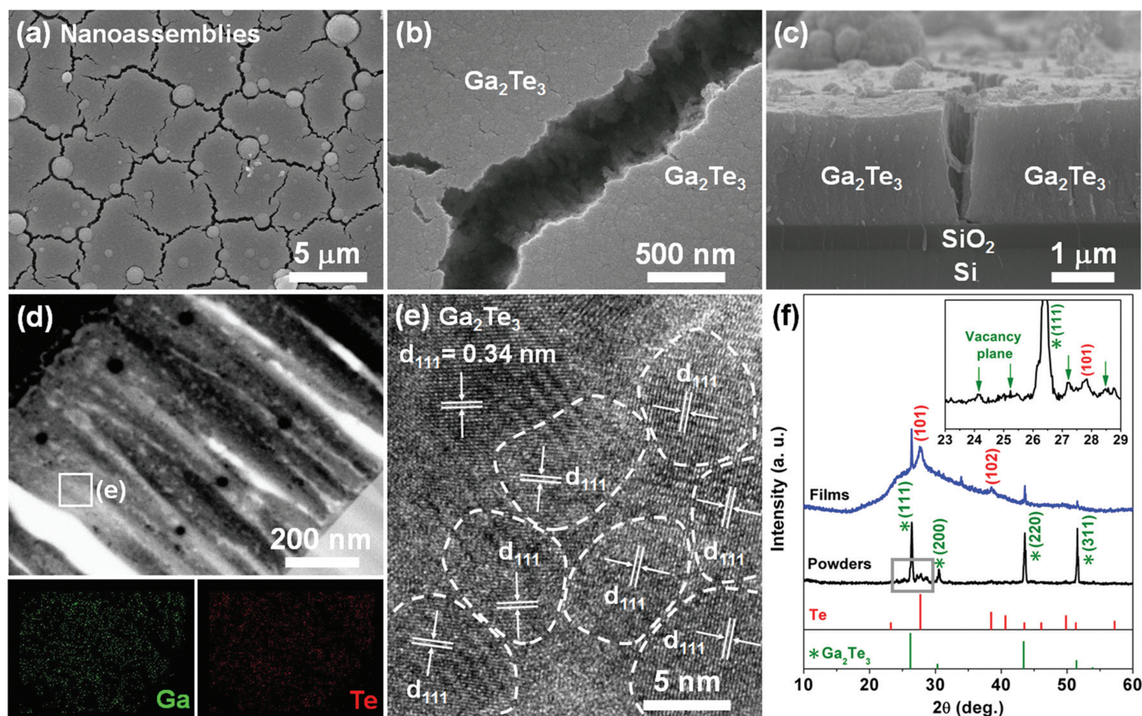

Fig. 1 (a) The top-view SEM image of Ga_2Te_3 nanostructured films deposited at 25 °C, and the (b) top-view and (c) cross-sectional close-ups aiming at the spontaneously formed cracks. (d) The cross-sectional TEM image and the corresponding EDS elemental maps representing the spatial distribution of Ga and Te elements. (e) The HRTEM image taken from the square region marked in (d). (f) The XRD patterns of the as-deposited Ga_2Te_3 nanostructured film and its raw material. The cubic Ga_2Te_3 (JCPDS 35-1490) and hexagonal Te (JCPDS 01-0727) references are attached. Inset pattern proves the presence of characteristic 2-D vacancy planes in Ga_2Te_3.

that were spontaneously formed just after the deposition procedure to relax the thermally induced internal tensile stresses in the prepared film. The XRD pattern, which can be conclusively indexed as cubic Ga_2Te_3 (JCPDS 35-1490) and hexagonal Te (JCPDS 01-0727), confirms the co-existence of stoichiometric Ga_2Te_3 and traceable secondary phase Te (Fig. 1f). The atomic ratio of Te/Ga that can be quantitatively determined from the EDS spectra is ~2.0, which significantly exceeds the stoichiometric value of 1.5. Although the great excess in the Te component should originate from the large loss of lighter Ga species (excited atoms and ions) when laser ablation was performed, significant Te agglomerates are absent, according to the TEM elemental mapping of the Ga and Te elements (Fig. 1d). This type of component separation may not be the mere case, in particular for the tellurium relevant PLD films, namely, Bi_2Te_3;[23,24] however, This must be the first time that it has been considered to be a very crucial step in creating the following novel heterogeneous Ga_2Te_3/Te nanostructures. In addition to the sharper XRD peaks, an unusually broad and massive band, coincidently covering the characteristic diffraction peaks of both phases, suggests that amorphous matter or extremely tiny crystals might simultaneously form at such a low deposition temperature (Fig. 1f). The present as-deposited film, containing a number of Ga_2Te_3/Te nanoassemblies isolated by interlocking cracks, becomes the most versatile original template for developing the desired advance heterogeneous nanocomposites.

Fig. 2a–c demonstrate amazing changes in the morphologies when the as-deposited Ga_2Te_3/Te nanoassembled film was annealed at 225 °C for 12 h. As can be seen, the wedge-shaped cracks are fully and even over filled with another phase, which can be clearly identified as a pure Te phase by comparing the TEM image and elemental mappings (Fig. 2d). The perfect TEM lattice fringes of the selected zone (f) (in Fig. 2d) provide further evidence that the appeared Te phase is a single crystalline (Fig. 2f). The corresponding fast Fourier-transform electron diffraction (FFT ED) analysis (zone axis = [010]) indicates that the Te single crystal is [101] oriented normally to the substrate. The EDS atomic ratio of Te/Ga found from the Ga_2Te_3 nanoassembly drastically decreases from ~2.0 of the as-deposited film to ~1.5 of the annealed one, confirming the outward diffusion of the Te component from the as-deposited Te embedded Ga_2Te_3 nanoassembly. A less significant structural change in the Ga_2Te_3 nanoassembly has been found, (Fig. 2e) although the embedded Te component is approximately absent. The primary phase, namely, each isolated Ga_2Te_3 nanoassembly (size ~3 μm on average) closely cooperates with the secondary phase, which is the interlocking Te single crystal (width ~0.5 μm), to spontaneously form an excellent heterogeneous nanocomposite with a very short phase alternating period (~3.5 μm) along the lateral (in-plane) direction. It is worth noting that the present innovative laterally assembled Ga_2Te_3/Te nanocomposite film contains a high density of not only the greatly regular Ga_2Te_3/

 This journal is © The Royal Society of Chemistry 2014

Published on 29 September 2014. Downloaded by National Chiao Tung University on 21/07/2015 10:47:55.

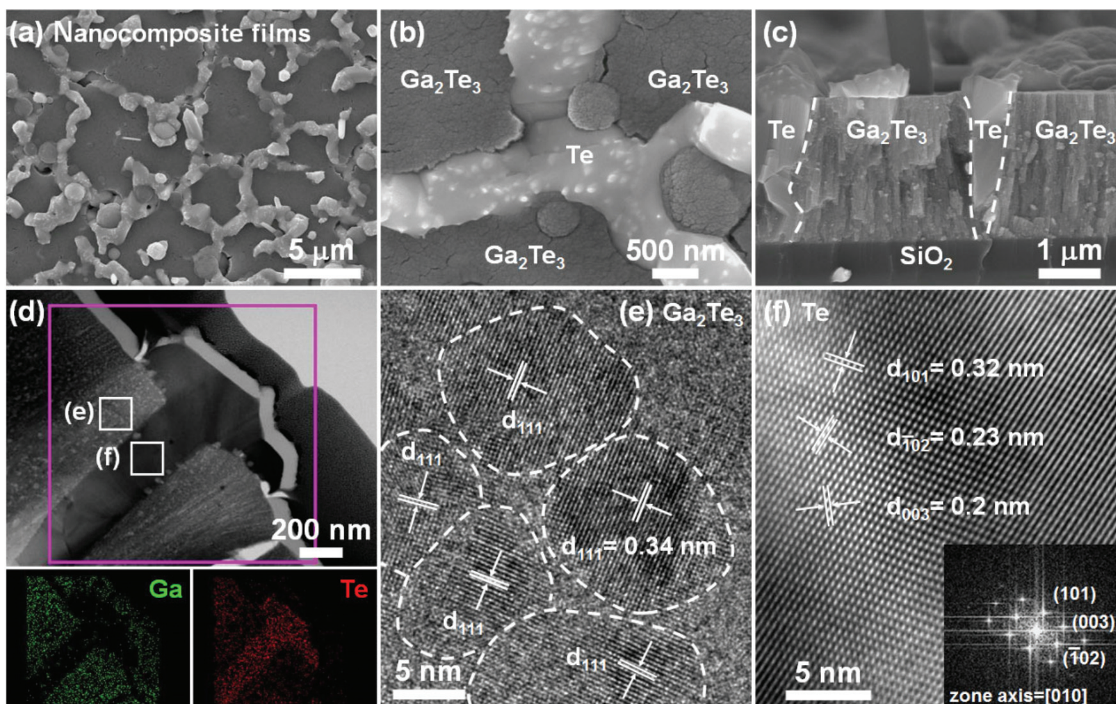

Fig. 2 (a) The top-view SEM image of the laterally-assembled Ga_2Te_3/Te hetero-nanocomposite film formed at an annealing temperature of 225 °C for 12 h. The magnified (b) top-view and (c) cross-sectional SEM images confirm that the V-cracks are completely occupied with Te. (d) The cross-sectional TEM image and the corresponding sharp EDS elemental maps further prove the presence of pure Te in the cracks. The HRTEM images of (e) the Ga_2Te_3 and (f) the Te sampling from the marked regions shown in (d). Inset in (f) shows the corresponding FFT ED pattern.

Te heterogeneous interfaces, but also the Ga_2Te_3/Ga_2Te_3 homogeneous ones for probably scattering phonons with various mean free paths. More importantly, the Te single-crystalline networks provide special channels for charged carriers to suppress the interfacial effects on lowering the electrical conductivity. The corresponding compositional line scans and TEM-EDS spectra are shown in Fig. S1.† In addition to the hetero-nanocomposite films prepared at 225 °C for 12 h, we have also systematically investigated the specimen annealed at 250 °C and 200 °C for 3 h, as can be seen in Fig. S2 and S3,† respectively.

To clarify the effects of annealing temperature and time, various annealing conditions were applied to the as-deposited Ga_2Te_3/Te films. As displayed in Fig. 3, both the factors would result in obvious changes in the morphology as well as the amount of the re-grown Te single crystals; therefore, they would directly govern the interfacial structure and the resulting thermoelectric properties. The re-grown Te crystal obtained at 175 °C (Fig. 3a) and at higher temperatures (Fig. 3b–e) is respectively ruled by an isolated one-dimensional and interlocking three-dimensional growth model. A closer look at Fig. 3a reveals numerous Te nanorods sticking out from the cracked surface, and more specially, directly penetrating two neighbouring Ga_2Te_3 nanoassemblies as a bridge. When the annealing temperature rises to 200 °C, which is almost half of the Te melting point (~450 °C for bulk[25]), the drastically enhanced Te diffusion in and on the Ga_2Te_3 nanoassemblies speeds up the Te growth to gradually fill the crack leading to a partially filled morphology (Fig. 3b). The optimized annealing condition should be 225 °C and 3 h because the re-grown Te crystals just fully fill the crack to leave a relatively smooth surface (Fig. 3c), which is of importance for further processes and applications, in contrast to the over-filled case obtained at the same temperature but for a much longer time of 12 h (Fig. 3e). Surprisingly, as the temperature increased to 250 °C, only a small quantity of the Te precipitate was formed in the cracks leaving a semi-filled morphology (Fig. 3d). The morphological variety of the films formed at an annealing temperature range from 150 °C to 275 °C for 3 h and 12 h are shown in Fig. S4 and S5,† respectively.

The EDS analyses focusing on the annealed Ga_2Te_3 nanoassemblies (Fig. 3f) clearly show a decreasing trend in the Te atomic fraction with the annealing temperature and time. Concerning the initial Te atomic fraction of ~66% measured from the as-deposited Ga_2Te_3 nanoassemblies, the degree of the lost Te component is basically in agreement with the level of the re-grown Te crystal found in the SEM images, excluding the case of 250 °C for 3 h. We believe that during the annealing process, the Te component would diffuse outwards from the Ga_2Te_3 nanoassemblies to the cracks and then simultaneously evaporate, in particular at the highest temperature of 250 °C. In addition, when the Ga_2Te_3 nanoassemblies were annealed at 225 °C for 12 h, the Te atomic fraction approximately approached the stoichiometric value of Ga_2Te_3 (Te: 60 at%). According to the Ga-Te equilibrium phase diagram,[17,25] it is believed that the pure Te component

Published on 29 September 2014. Downloaded by National Chiao Tung University on 21/07/2015 10:47:55.

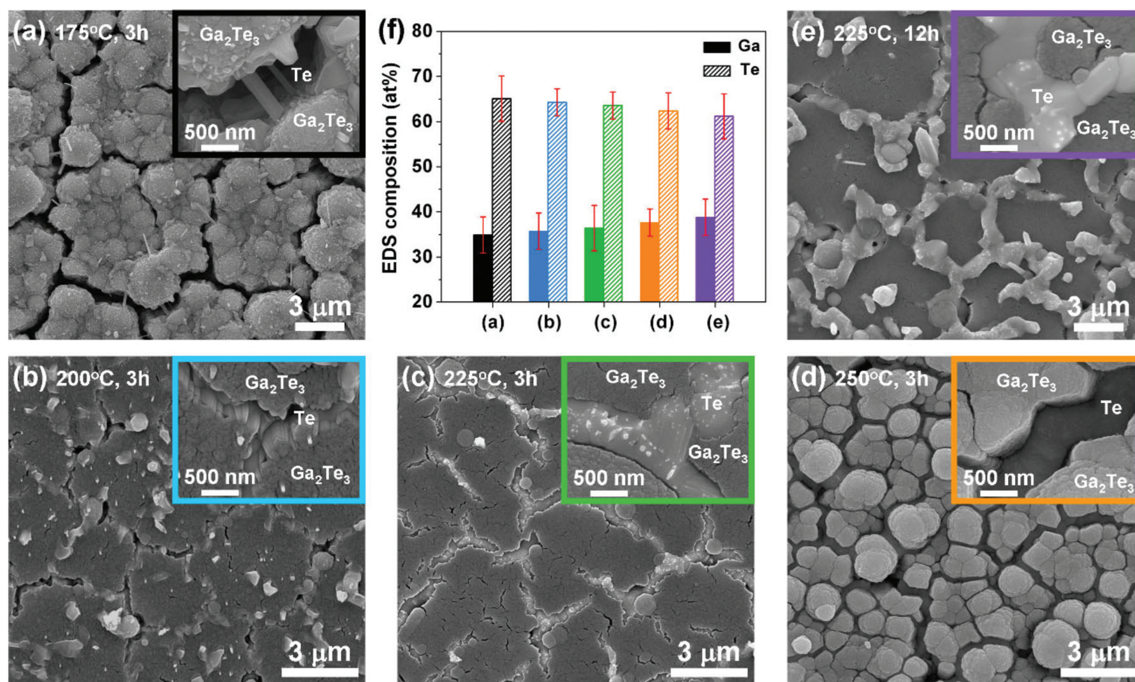

Fig. 3 The top-view SEM images of the Ga_2Te_3/Te hetero-nanocomposite films prepared at (a) 175 °C for 3 h, (b) 200 °C for 3 h, (c) 225 °C for 3 h, (d) 250 °C for 3 h, and (e) 225 °C for 12 h. Insets show the close-up of the occupancy condition of Te. (f) The corresponding EDS compositional analyses aimed at the Ga_2Te_3 nanoassemblies.

might be completely transferred from the Ga_2Te_3 nanoassemblies to the cracks to leave the over-filled morphology (Fig. 3e). The detailed EDS spectra acquired from SEM are displayed in Fig. S6.†

Fig. 4a shows the XRD patterns of the annealed Ga_2Te_3/Te nanocomposite films. The very broad band displayed in Fig. 1f was entirely replaced with a strong and sharp Te (101) peak for all the annealed films, excluding the one at 175 °C. It is thus believed that a great amount of extremely tiny Te clusters should exist in the as-deposited Ga_2Te_3 nanoassemblies to contribute to the very strong and broad band (Fig. 1f). The residual broad band for 175 °C is in good agreement with the less-formed Te nanorods (Fig. 3a). The relatively strong Te (101) peaks confirm the (101) oriented growth normal to the substrate (Fig. 2f). The detailed XRD patterns of the hetero-nanocomposite films formed at an annealing temperature range from 150 °C to 275 °C for 3 h and 12 h are shown in Fig. S7 and S8,† respectively.

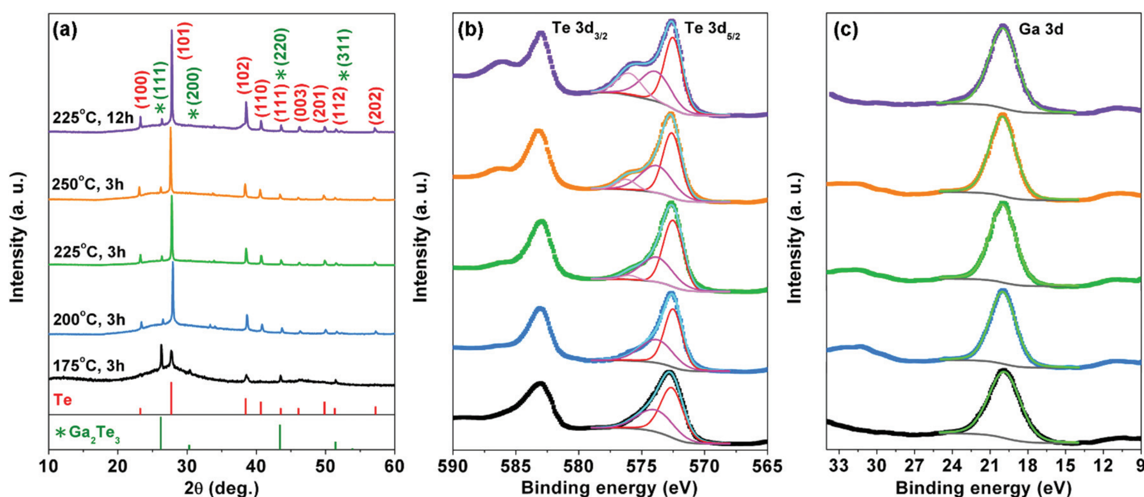

Fig. 4 (a) The XRD patterns of the laterally-assembled Ga_2Te_3/Te hetero-nanocomposite films prepared at various annealing conditions. The large-area XPS analyses of (b) Te 3d and (c) Ga 3d. The asymmetric Te $3d_{5/2}$ spectra are mainly composed of Te^{2+} (572.5 eV) of Ga_2Te_3, Te^0 (573.8 eV), and Te^{4+} (576.5 eV) of TeO_2. The symmetric Ga 3d profile is consistent with Ga^{3+} (19.9 eV) of Ga_2Te_3.

This journal is © The Royal Society of Chemistry 2014

Published on 29 September 2014. Downloaded by National Chiao Tung University on 21/07/2015 10:47:55.

Fig. 4b and 4c *show the* XPS analysis around Te 3d and Ga 3d, respectively. In the cases of 175 °C and 200 °C, the Te $3d_{5/2}$ peak can be reasonably decomposed into two components. The stronger peak at 572.5 eV corresponds to the negatively charged Te from Ga_2Te_3, whereas the side peak at 573.8 eV is assigned to the uncharged metallic Te. Moreover, in the case of 225 °C (3 h and 12 h) and 250 °C, three components, which are respectively assigned to the negatively charged Te (572.5 eV) from Ga_2Te_3, uncharged metallic Te (573.8 eV), and positively charged Te (576.5 eV) from TeO_2, are required to have high quality fitting. The found binding energies are consistent with the reported literature.[26,27] The present result suggests that the TeO_2 fraction increases with the annealing temperature and also with time. The symmetric Ga 3d peaks can be well-fitted with a single peak at 19.9 eV agreeing with the literature value for Ga_2Te_3,[26] confirming the absence of the oxidation state (Fig. 4c).

Fig. 5 summarizes the five Te-filling models found in the Ga_2Te_3/Te nanocomposite films, along with the conclusive evidence. During laser ablation, a continuous film forms on the unheated substrate. Due to the thermal expansion mismatch, the film then immediately cools down and cracks when the supply of high-energy species ablated from the target is stopped.[23,24,28] This phenomenon was specially utilized to form specific interlocking crack templates in the as-deposited Ga_2Te_3 nanoassembled films required for creating the novel Ga_2Te_3/Te nanocomposite films. Comparing with the smooth top film surface, the very rough crack interfaces, composed of numerous Ga_2Te_3 nanograins, provide the nucleation sites needed for Te growth. At the beginning of the annealing

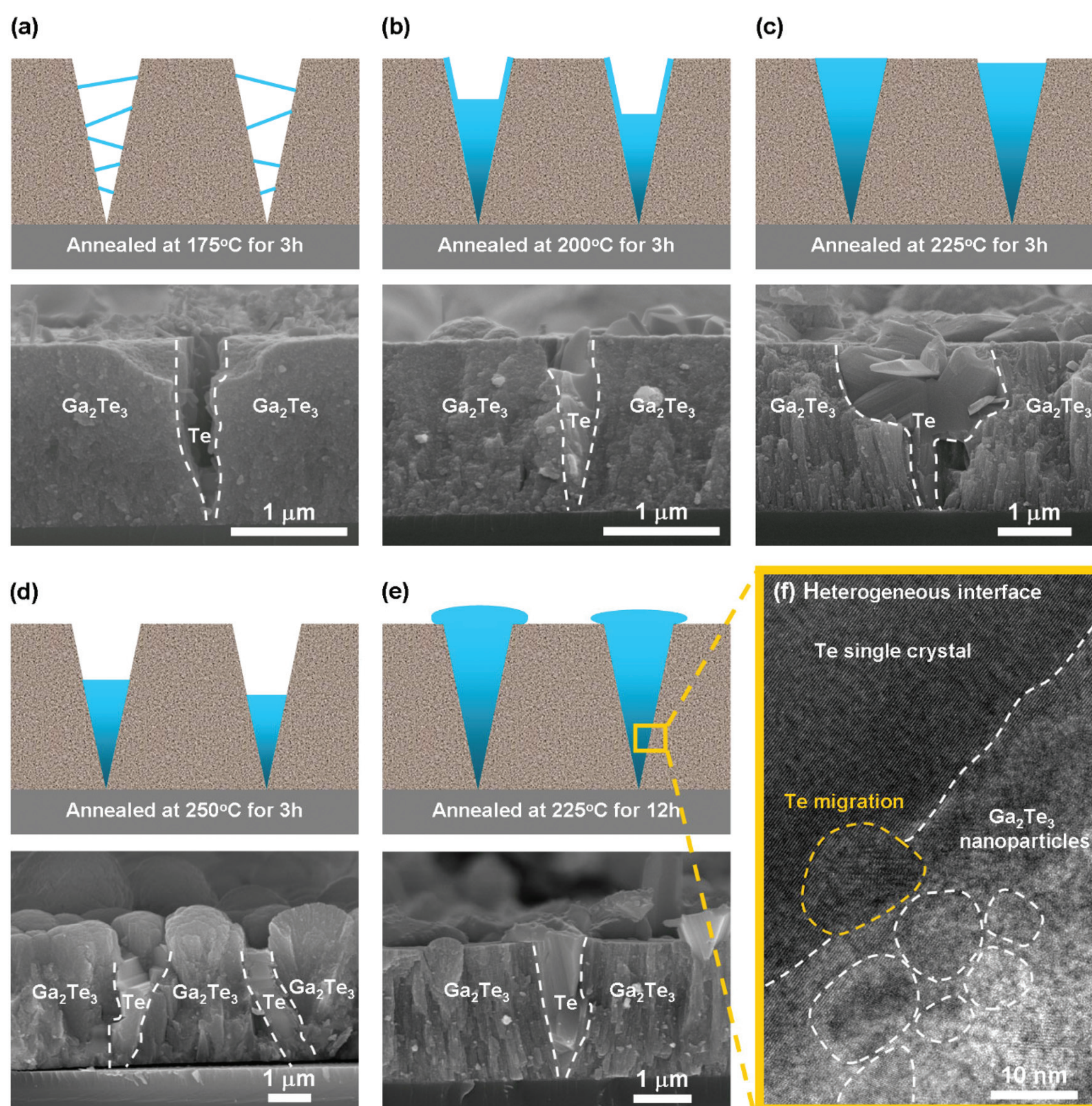

Fig. 5 Schematic diagrams and the corresponding SEM evidence summarizing the occupancy situation of Te at different annealing conditions: (a) 175 °C for 3 h, (b) 200 °C for 3 h, (c) 225 °C for 3 h, (d) 250 °C for 3 h, and (e) 225 °C for 12 h. (f) The HRTEM image taken from the Ga_2Te_3/Te hetero-interface is marked in (e).

Published on 29 September 2014. Downloaded by National Chiao Tung University on 21/07/2015 10:47:55.

treatment, a large number of Te nuclei precipitate from the Ga_2Te_3 nanoassembled matrix, and then the crystal nuclei keep growing by continuously absorbing the outward diffusing Te atoms. The required temperature for Te growth is found to be above 150 °C for 3 h. Because the annealing temperature approaches approximately half of the melting point, the Te grains might coarsen to form an entire single-crystalline interlocking by sacrificing smaller grains to decrease the total interfacial area and hence the free energy.[29] As can be observed in the lattice image (Fig. 5f), one small Te grain was just trapped at the Ga_2Te_3/Te interface, which might provide evidence of the progress of Te migration and grain coarsening. A similar precipitate reaction has also been found in Bi_2Te_3/Te multiple heterostructure nanowires.[29] In addition, we also found a thin Te coating on the un-filled crack surface, as illustrated in Fig. 5b, which might suggest that Te would diffuse from the upper crack surface to the bottom to form a larger crystal.

Fig. 6 shows a set of in-plane thermoelectric properties obtained from the laterally assembled Ga_2Te_3/Te nanocomposite films. Hall measurements confirm that holes are the majority carriers for all the specimens. The carrier concentration significantly increases with the annealing temperature for both the series of 3 h and 12 h, and respectively reaches the highest value of 6.1×10^{17} cm^{-3} (225 °C) and 2.3×10^{17} cm^{-3} (250 °C) (Fig. 6a), approximately 100-fold higher than the literature value for Ga_2Te_3 films ($\sim 5 \times 10^{15}$ cm^{-3}).[30] The corresponding mobility can also approach a very high level of 27 cm^2 V^{-1} s^{-1} (225 °C for 3 h) and 42 cm^2 V^{-1} s^{-1} (225 °C for 12 h), which is considerably above the reported values, for example, the Te films (0.032 cm^2 V^{-1} s^{-1})[21] and the Ga_2Te_3 films (7 cm^2 V^{-1} s^{-1}).[30]

The tendency shown in Fig. 6b evidently concludes that the electrical conductivity is basically dominated by the Te-filling fraction in the cracks due to the correspondingly created single-crystalline channels for the carriers. However, two data points, 225 °C and 250 °C for 3 h, appear to deviate from the uprising tendency probably due to the formation of the TeO_2 (Fig. 4b). It is worth noting that the highest electrical conductivity (177 S m^{-1}) is 2 to 3 orders higher than that of the Ga_2Te_3 bulk (0.5 S m^{-1}),[18] Ga_2Te_3 films (0.5 S m^{-1}),[30] and Te films (4 S m^{-1})[21] at room temperature, confirming that the single-crystalline Te filled cracks between the Ga_2Te_3 nanoassemblies can effectively enhance the carrier mobility as well as the electrical conductivity.

The positive Seebeck coefficients for all the specimens indicate p-type semiconducting behaviour, as concluded by the Hall measurement, and steadily reduce with increasing annealing temperature (see Fig. S9 and S10†). The relation between the Seebeck coefficient and annealing time might be understandable as the reason for the tendency in Fig. 6b. The maximum Seebeck coefficient of 525 μV K^{-1} (150 °C for 3 h and 12 h) as well the optimized 332 μV K^{-1} (225 °C for 3 h), which would lead to the highest power factor (Fig. 6d), are above that of the Te films (290 μV K^{-1} at 300 K)[21] but lower

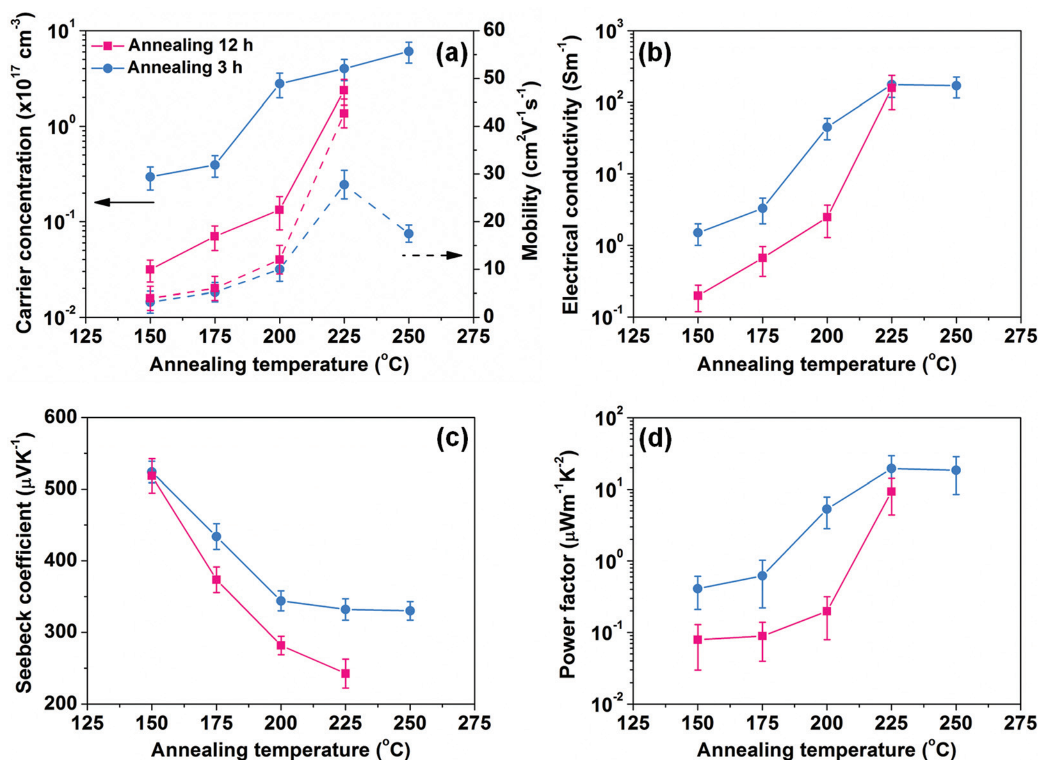

Fig. 6 The in-plane thermoelectric properties of the laterally-assembled Ga_2Te_3/Te hetero-nanocomposite films. (a) The carrier concentration (solid line) and mobility (dash line), (b) the electrical conductivity, (c) the Seebeck coefficient, and (d) the power factor as functions of annealing temperatures.

 This journal is © The Royal Society of Chemistry 2014

Published on 29 September 2014. Downloaded by National Chiao Tung University on 21/07/2015 10:47:55.

than that of the Ga_2Te_3 bulk (800 μV K^{-1} at 300 K)[18] at room temperature. The corresponding power factors (Fig. 6d) exhibit a similar tendency to the electrical conductivity (Fig. 6c). Surprisingly, the highest power factor of 19.5 μW m^{-1} K^{-2} obtained is 60-fold higher than the values of the Ga_2Te_3 bulk (0.32 μW m^{-1} K^{-2})[18] and the Te films (0.34 μW m^{-1} K^{-2})[21] at room temperature. In particular, it is noteworthy that this value is comparable to the best room-temperature material systems, such as Ag_xTe_y/Sb_2Te_3 films (20–102 μW m^{-1} K^{-2}),[14] Pt/Sb_2Te_3 films (102 μW m^{-1} K^{-2}),[13] and Te/Bi_2Te_3 bulk (112 μW m^{-1} K^{-2}),[9] indicating that the present laterally assembled Ga_2Te_3/Te nanocomposite films would be one of the promising options for developing low-temperature thermoelectric materials.

To obtain reliable cross-sectional thermal conductivity, the well-developed 3ω technique[31,32] was utilized for the laterally assembled Ga_2Te_3/Te nanocomposite films at room temperature. The Te fully-filled specimen (225 °C for 3 h) exhibits a cross-plane thermal conductivity of around 0.68 ± 0.03 W m^{-1} K^{-1}, which is just slightly higher than 0.5 W m^{-1} K^{-1} for the Ga_2Te_3 bulk,[18] obviously due to the presence of the highly-conductive Te single crystals (the reported thermal conductivity of the Te bulk is ~3 W m^{-1} K^{-1})[33] in the present film system.

The present results provide evidence that the laterally assembled Ga_2Te_3/Te nanocomposite films, in particular the Te fully-filled type (225 °C for 3 h), not only exhibit the excellent power factor of ~19.5 μW m^{-1} K^{-2}, but displays the desired low cross-plane thermal conductivity of 0.68 W m^{-1} K^{-1}. The concept of introducing multiple functional interfaces has been achieved in the laterally assembled Ga_2Te_3/Te nanocomposite films *via* precisely controlled PLD techniques followed by annealing processes.

Conclusions

An interfacial concept of laterally alternated nanocomposite films, coupling isolated p-type Ga_2Te_3 assemblies and interlocking p-type Te single crystals, has been proposed and successfully achieved using PLD techniques and subsequent annealing processes. By precisely controlling the crucial factors of temperature and time, the supersaturated Te clusters that are uniformly dispersed in the as-deposited Ga_2Te_3 films would dynamically diffuse outwards and accordingly grow to present various styles of filling morphologies in the spontaneously formed thermal cracks that are perpendicular to the substrate.

The obtained laterally assembled Ga_2Te_3/Te nanocomposite films contain multiple high-density periodical interfaces, including the naturally formed 2-D vacancy planes in each Ga_2Te_3 nanocrystal (atomic-scale), the homogeneous interfaces between Ga_2Te_3 nanograins (nano-scale), and the Ga_2Te_3/Te heterogeneous interfaces (meso-scale). The single-crystalline Te 2-D net acts to be an alternative channel for transporting carriers to reduce the induced high resistance of the interfaces. Due to the comprehensively modulated approach, the present nanocomposite films exhibit an unexpectedly low thermal conductivity of 0.68 W m^{-1} K^{-1}, while a comparably high electrical conductivity of 177 S m^{-1} is retained. Accompanying the high-level Seebeck coefficient (332 μV K^{-1}), the excellent power factor (19.5 μW m^{-1} K^{-2}) was thus achieved.

Acknowledgements

This work was supported by the National Science Council of the Republic of China under grant NSC-101-2221-E-009-045-MY2 and NSC-100-2221-E-009-023-MY3. The authors are grateful to Professor Mei-Jiau Huang at National Taiwan University and Dr. Heng-Chieh Chien at Industrial Technology Research Institute for their insightful discussion.

Notes and references

1 D. L. Medlin and G. J. Snyder, *Curr. Opin. Colloid Interface Sci.*, 2009, **14**, 226.
2 K. Nielsch, J. Bachmann, J. Kimling and H. Böttner, *Adv. Energy Mater.*, 2011, **1**, 713.
3 Y. Zhang and G. D. Stucky, *Chem. Mater.*, 2014, **26**, 837.
4 K. Biswas, J. He, I. D. Blum, C. I. Wu, T. P. Hogan, D. N. Seidman, V. P. Dravid and M. G. Kanatzidis, *Nature*, 2012, **489**, 414.
5 J. M. O. Zide, D. Vashaee, Z. X. Bian, G. Zeng, J. E. Bowers, A. Shakouri and A. C. Gossard, *Phys. Rev. B: Condens. Matter*, 2006, **74**, 205335.
6 S. V. Faleev and F. Léonard, *Phys. Rev. B: Condens. Matter*, 2008, **77**, 214304.
7 A. Popescu, L. M. Woods, J. Martin and G. S. Nolas, *Phys. Rev. B: Condens. Matter*, 2009, **79**, 205302.
8 J. Zhou, X. Li, G. Chen and R. Yang, *Phys. Rev. B: Condens. Matter*, 2010, **82**, 115308.
9 G. Zhang, H. Fang, H. Yang, L. A. Jauregui, Y. P. Chen and Y. Wu, *Nano Lett.*, 2012, **12**, 3627.
10 L. Cheng, Z. G. Chen, L. Yang, G. Han, H. Y. Xu, G. J. Snyder, G. Q. Lu and J. Zou, *J. Phys. Chem. C*, 2013, **117**, 12458.
11 H. Lu, P. G. Burke, A. C. Gossard, G. Zeng, A. T. Ramu, J. H. Bahk and J. E. Bowers, *Adv. Mater.*, 2011, **23**, 2377.
12 S. Sumithra, N. J. Takas, D. K. Misra, W. M. Nolting, P. F. P. Poudeu and K. L. Stokes, *Adv. Energy Mater.*, 2011, **1**, 1141.
13 D. K. Ko, Y. Kang and C. B. Murray, *Nano Lett.*, 2011, **11**, 2841.
14 Y. Zhang, M. L. Snedaker, C. S. Birkel, S. Mubeen, X. Ji, Y. Shi, D. Liu, X. Liu, M. Moskovits and G. D. Stucky, *Nano Lett.*, 2012, **12**, 1075.
15 K. C. See, J. P. Feser, C. E. Chen, A. Majumdar, J. J. Urban and R. A. Segalman, *Nano Lett.*, 2010, **10**, 4664.
16 M. He, J. Ge, Z. Lin, X. Feng, X. Wang, H. Lu, Y. Yang and F. Qiu, *Energy Environ. Sci.*, 2012, **5**, 8351.

Published on 29 September 2014. Downloaded by National Chiao Tung University on 21/07/2015 10:47:55.

17 M. Guymont, A. Tomas and M. Guittard, *Philos. Mag. A*, 1992, **66**, 133.
18 K. Kurosaki, H. Matsumoto, A. Charoenphakdee, S. Yamanaka, M. Ishimaru and Y. Hirotsu, *Appl. Phys. Lett.*, 2008, **93**, 012101.
19 C. E. Kim, K. Kurosaki, M. Ishimaru, H. Muta and S. Yamanaka, *J. Electron. Mater.*, 2011, **40**, 999.
20 V. D. Das, N. Jayaprakash and N. Soundararajan, *J. Mater. Sci.*, 1981, **16**, 3331.
21 V. T. Division, *Phys. Status Solidi*, 1983, **77**, K81.
22 M. A. Dinno, M. Schwartz and B. Giammara, *J. Appl. Phys.*, 1974, **45**, 3328.
23 A. Bailini, F. Donati, M. Zamboni, V. Russo, M. Passoni, C. S. Casari, A. L. Bassi and C. E. Bottani, *Appl. Surf. Sci.*, 2007, **254**, 1249.
24 H. C. Chang and C. H. Chen, *CrystEngComm*, 2011, **13**, 5956.
25 Y. Feutelais and B. Legendre, *Thermochim. Acta*, 1998, **314**, 35.
26 E. G. Gillan and A. R. Barron, *Chem. Mater.*, 1997, **9**, 3037.
27 S. Xu, C. Wang, R. Wang, Z. Wang, Q. Xu and Y. Cui, *J. Mater. Chem.*, 2011, **21**, 1647.
28 M. N. R. Ashfold, F. Claeyssens, G. M. Fuge and S. J. Henley, *Chem. Soc. Rev.*, 2004, **33**, 23.
29 W. Wang, X. Lu, T. Zhang, G. Zhang, W. Jiang and X. Li, *J. Am. Chem. Soc.*, 2007, **129**, 6702.
30 K. George, C. H. D. Groot, C. Gurnani, A. L. Hector, R. Huang, M. Jura, W. Levason and G. Reid, *Chem. Mater.*, 2013, **25**, 1829.
31 T. Yamane, N. Nagai, S. Katayama and M. Todoki, *J. Appl. Phys.*, 2002, **91**, 9772.
32 H. C. Chang, C. H. Chen and Y. K. Kuo, *Nanoscale*, 2013, **5**, 7017.
33 C. Y. Ho, R. W. Powell and P. E. Liley, *J. Phys. Chem. Ref. Data*, 1972, **1**, 279.

 This journal is © The Royal Society of Chemistry 2014